Lab on a Chip

PAPER

View Article Online
View Journal | View Issue

Cite this: *Lab Chip*, 2025, **25**, 6335

Microfluidic device for islet conformal coating with a polyethylene glycol-based hydrogel: innovating cell immunoprotection strategies in type 1 diabetes

Francesca Vicinanza, †[a] Tatiana Mencarini, †[a] Francesca Verderio,[a] Grisell C. Gonzalez, [b] Helena Montuoro,[a] Silvia Bozzi,[a] Ashutosh Agarwal, [cd] Marco Rasponi, [a] Alberto Redaelli *[a] and Alice A. Tomei *[bcef]

Microencapsulation of therapeutic cell clusters within immunoprotective hydrogels is a key strategy in endocrine, hepatic, neural, and musculoskeletal regenerative medicine. Conformal hydrogel coating (CC) of pancreatic islets represents a promising approach for β cell replacement in type 1 diabetes (T1D), offering immunoprotection to prevent rejection. However, current CC techniques are limited by poor scalability, complex workflows, and high reagent use. Here, we present a flow-focusing soft lithographic microfluidic platform that enables thin polyethylene glycol (PEG)-based CC around insulin-secreting cell clusters in a tunable and scalable manner. The device employs three immiscible phases—an aqueous PEG precursor, an oil sheath, and an external cross-linking emulsion—configured to achieve 10–20 μm coating thicknesses. Both murine insulinoma pseudoislets and primary human islets were encapsulated and assessed for coating dimensions, viability, and glucose-stimulated insulin secretion (GSIS). The platform reliably generated CC with thickness independent of cluster size. Fluorescent labeling of PEG coatings and confocal imaging confirmed complete and uniform coverage. Encapsulated clusters retained high viability and GSIS functionality. The system achieved a >10–100-fold reduction in graft volume relative to conventional microencapsulation, potentially expanding implantation site options. The process maintains physiological pH throughout encapsulation, a condition known to support cell health and reduce stress-induced damage. In addition, the streamlined workflow reduces processing time and simplifies operation compared to previous CC approaches. Overall, this work introduces a robust, low-footprint, and adaptable microfluidic strategy for conformal coating of cell clusters, offering a scalable platform for immunoisolated therapeutic cell transplantation in T1D and broader regenerative medicine applications.

Received 11th July 2025,
Accepted 13th October 2025

DOI: 10.1039/d5lc00690b

rsc.li/loc

1 Introduction

In the past decades, hydrogel-based microencapsulation has emerged as a versatile technology for therapeutic cell delivery with applications across drug delivery, tissues engineering and regenerative medicine,[1–3] including the treatment of a wide range of diseases and injuries such as neurodegenerative disorders, diabetes, cardiovascular and liver diseases, musculoskeletal defects, osteoarthritis, and wound healing. Hydrogels are ideal materials for cell-based therapies to protect cells or bioactive agents within a soft, biocompatible, and highly hydrated matrix. A wide variety of natural and protein-derived polymers—such as alginate, agarose, hyaluronic acid, collagen, and gelatin—have been used to form hydrogel capsules around therapeutic cell clusters through techniques that include emulsification, bioprinting, and microfluidics.[4,5]

Within this broader context, islet cell encapsulation has risen as a promising strategy to advance β cell replacement therapies for type 1 diabetes (T1D). T1D is a chronic autoimmune disease characterized by the destruction of insulin-producing β cells in the pancreas.[6,7] While exogenous

[a] *Department of Electronics, Information and Bioengineering, Politecnico di Milano, Milan, Italy. E-mail: alberto.redaelli@polimi.it*
[b] *Diabetes Research Institute, University of Miami Miller School of Medicine, Miami, FL-33136, USA. E-mail: atomei@med.miami.edu*
[c] *Department of Biomedical Engineering, University of Miami, Miami, FL-33146, USA*
[d] *Desai Sethi Urology Institute, University of Miami Miller School of Medicine, Miami, Florida 33136, USA*
[e] *Department of Surgery, University of Miami Miller School of Medicine, Miami, FL-33136, USA*
[f] *Department of Microbiology and Immunology, University of Miami Miller School of Medicine, Miami, FL-33136, USA*
† These authors contributed equally to this work.

insulin administration is the standard therapy, it fails to fully mimic the dynamic insulin secretion of native islets, often resulting in suboptimal glycemic control and long-term complications.[8] Allogeneic islet transplantation offers a promising curative approach by restoring endogenous insulin secretion, improving metabolic control, and enhancing patient quality of life.[9,10] However, besides the scarce availability of donors, its clinical implementation is limited by the need for lifelong systemic immunosuppression, which poses significant risks such as nephrotoxicity, opportunistic infections, and increased malignancy rates.[11–14]

To circumvent this limitation, immunoisolation strategies such as islet encapsulation have been extensively explored.[15] These approaches aim to create a selectively permeable barrier around transplanted cells that permits the bidirectional diffusion of glucose, insulin, oxygen, nutrients, and waste products, while blocking immune system components.[16] Conventional encapsulation methods, including macro- and micro-encapsulation, generally using alginate or polyethylene glycol (PEG)-based hydrogels, have shown some success in protecting islets from immune rejection.[17] Additionally, encapsulation is compatible with not only cadaveric islets but also alternative insulin-secreting cell sources such as stem cell-derived islets or porcine islets, helping to overcome the critical islet donor shortage.[18] Recently it has been demonstrated that the hydrogel shell can be functionalized thus enhancing engraftment and immune modulation by incorporating extracellular matrix proteins lost during islet isolation, angiogenic factors like vascular endothelial growth factor to promote revascularization, or nanomaterial-based systems for local delivery of anti-inflammatory and immunosuppressive agents.[19,20] However, these methods typically produce capsules of fixed, large diameter—often exceeding 500 μm—which far surpasses the maximum effective diffusion distance for oxygen and nutrients (~150 μm),[21] particularly in avascular environments. These approaches result in hypoxia-induced islet dysfunction or necrosis and limit the choice of implantation sites to large, poorly vascularized cavities such as the peritoneum.

De Toni *et al.* reported that alginate microcapsules often reach 600–800 μm in diameter, with shell thicknesses ranging from a few micrometres to more than 700 μm. Increasing the thickness of the capsules slows islet responses to glucose stimulation, with *in vitro* perfusion assays showing up to ~5 min delays and reduced high glucose stimulation response peak by around 30%. *In silico* models predicted peak delays of up to about 15 min with impaired shutdown when lowering glucose challenge, and *in vivo* experiments confirmed prolonged hyperinsulinaemia. These findings highlight that capsule thickness, together with hydrogel formulation, is a critical limitation for maintaining physiological glucose–insulin dynamics.[22] To address this issue, conformal coating (CC) has recently emerged as a refined encapsulation strategy that addresses these drawbacks by forming a thin (typically 10–20 μm), uniform hydrogel layer that conforms to the natural shape and size of each islet.[23,24] This strategy drastically reduces the diffusion barrier and total transplant volume (*i.e.* graft volume), enabling islet transplantation in smaller, more vascularized sites such as the momentum and the subcutaneous space.[25–27]

Two main CC approaches have emerged: layer-by-layer (LbL) polymer assembly and hydrogel-based emulsion coating. The LbL techniques enable nanoscale control of coating thickness.[28–30] However, they are often limited by slow, labor-intensive protocols, and repeated handling steps that can compromise the integrity and viability of cell clusters. Additionally, many LbL coatings rely on polycationic materials which can destabilize the negatively charged cell membrane, leading to cytotoxicity and impaired cell function.[31] A further limitation is that these nanocoatings often fail to achieve complete or stable coverage of the cell surface, necessitating the co-delivery of immunosuppressive agents to achieve immunoprotection—suggesting that their physical barrier alone may be insufficient to shield transplanted cells from host immune attack.[32,33] In addition, LbL requires direct modification of islet cell surface and it is generally not stable since dependent on cell turnover.[34] More recently, flow-focusing emulsion-based CC methods, developed by our group, introduced a physiologically favorable pH environment during encapsulation, enhancing islet survival and demonstrating improved graft viability in preclinical models.[22,35,36]

In flow-focusing systems, two immiscible fluids are injected into the device. When the aqueous phase containing the polymer transitions from the dripping to the jetting regime, the interfacial tension between the two immiscible phases induces Plateau–Rayleigh instability, causing the polymer water phase stream to break up into discrete droplets.[37] This phenomenon is governed by the balance between the viscous shear stress of the continuous phase and the interfacial tension.[38]

When the aqueous polymer phase is loaded with particulates, the breakup of the jet leads to the formation of hydrogel shells around individual clusters. The presence of cell clusters within the flow increases local velocity and flow elongation, facilitating their separation and uniform coating.[23,39] These liquid capsules subsequently undergo gelation upon contact with a cross-linking emulsion that initiate polymerization.[35] This encapsulation mechanism enables precise spatial control of coating thickness while avoiding cluster aggregation, a key advantage over bulk encapsulation approaches.

In our previous works, conformal coating was performed using a machined macro-scale device. This consisted of a cylindrical oil chamber of about 10 mm in diameter into which the aqueous islet suspension was injected *via* a catheter. Downstream, a flow-focusing region tapered from 10 mm to 1 mm in diameter over a length of about 10 cm, followed by a 1 mm-diameter, 10 cm-long glass capillary where jet breakup and coating formation occurred.[40]

Despite the advantages, current CC techniques rely on bulky, complex systems with high reagent consumption, lack tunability of coating thickness, and they offer limited scalability. This limitation is particularly critical when considering that, for clinical translation, transplantation of approximately 10 000 islet equivalent (IEQ)—where 1 IEQ corresponds to the volume of a standard islet with a diameter of 150 μm[41]—per kilogram of recipient body weight is generally recommended as the minimal β cell mass required to achieve a meaningful metabolic effect.[13,42] Such benchmarks highlight the importance of developing encapsulation platforms that can be efficiently scaled toward clinical application. In recent years, microfluidic technologies have shown significant promise for generating uniform hydrogel-based capsules, in the context of conventional microencapsulation of islets or other cell types. Despite the widespread use of microfluidic platforms for microcapsule generation,[43–46] including systems with *in situ* gelation,[47–50] none, to the best of our knowledge, has been used for conformal coating generation.

In this work, we present the design and validation of a flow-focusing microfluidic platform that enables conformal coating of insulin-secreting cell clusters in a simple, scalable, and tunable manner. By finely tuning the relative flow rates of three immiscible streams—a central aqueous PEG hydrogel precursor containing the cell clusters, a surrounding coaxial oil sheath, an external cross-linking emulsion—we achieved consistent formation of thin hydrogel shells tightly adhering to the cluster surface. Unlike previous CC systems, our platform requires minimal reagent consumption, allows for real-time process monitoring, and can be readily adapted to accommodate clusters of varying size by altering channel cross-sections. This flexibility enables the encapsulation of both murine insulinoma clusters and human pancreatic islets, opening new avenues for cell-based therapies in T1D and beyond. Furthermore, our system preserves a physiological pH environment during encapsulation, enhancing cell viability and reducing the risk of inflammation associated with peripheral cell death.[35,51]

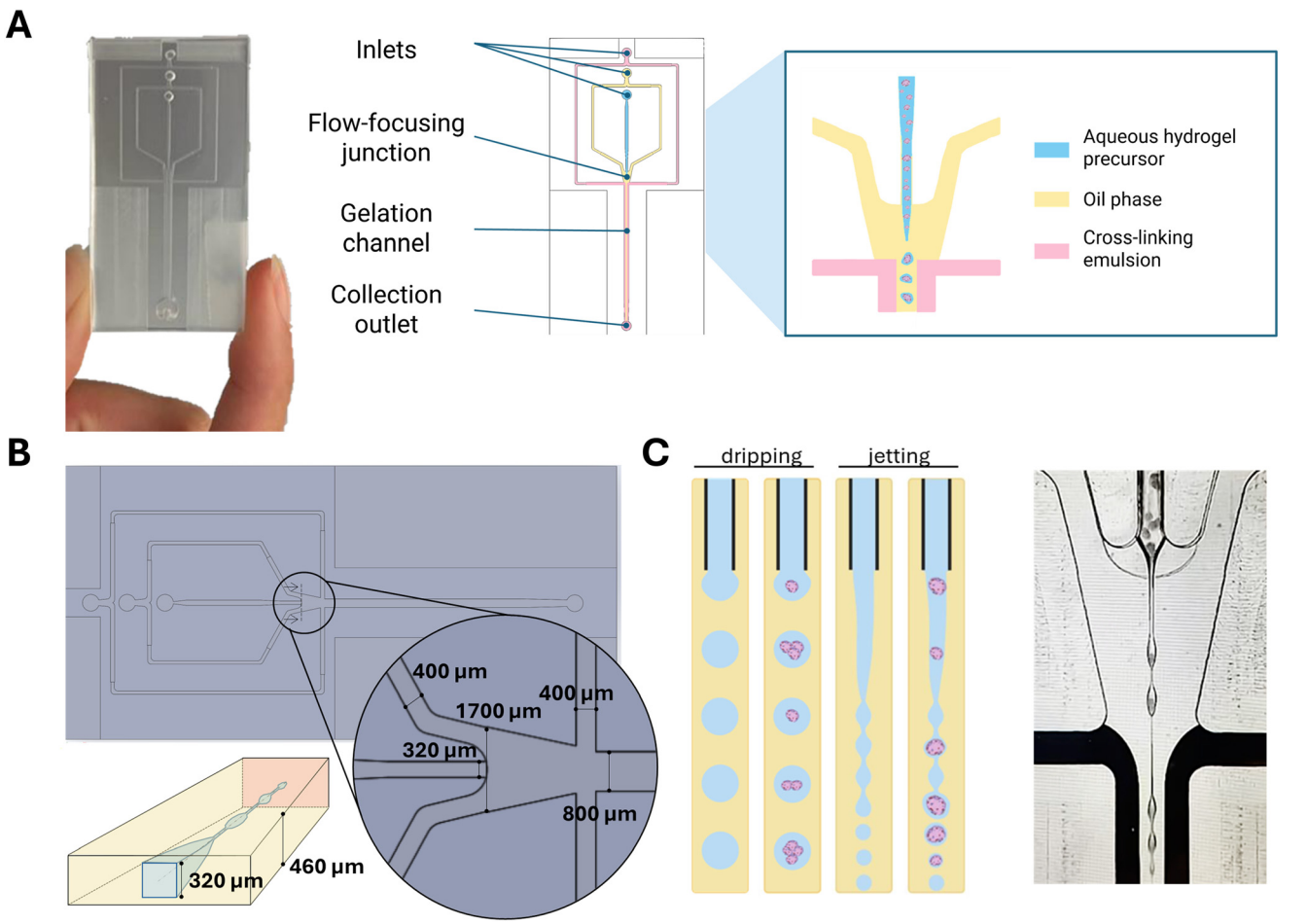

Fig. 1 Flow-focusing microfluidic platform for the conformal coating of insulin-secreting cell clusters. (A) Photograph of the microfluidic device (left) and schematic representation of its key features (right). Highlighted in the magnified schematic is the flow-focusing junction, where an aqueous phase containing the PEG hydrogel precursor solution and the cell clusters flows within an oil phase before entering in contact with the water-in-oil cross-linking emulsion phase. (B) Detailed design of the microfluidic junction, with channel dimensions. (C) Schematic illustration of the dripping and jetting regimes, alongside an experimental image showing the jetting regime with cell clusters suspended in the aqueous phase. Scale bar, 500 μm.

Through detailed characterization of flow conditions, coating uniformity, cell viability, and glucose-stimulated insulin secretion (GSIS), we demonstrate the feasibility and versatility of this microfluidic conformal coating approach. We propose it as a broadly applicable tool for cell encapsulation in regenerative medicine, enabling immunoprotection while preserving cell function and minimizing transplant burden. The microfluidic system presented here may serve as a proof of concept for a disposable encapsulation cartridge, potentially integrable into standardized clinical workflows and paving the way for scalable, streamlined cell-based therapies.

2 Materials and methods

2.1 Microfluidic platform design and dimensions

The microfluidic device was designed to enable the flow-focusing encapsulation of insulin-secreting cell clusters within a water-in-oil emulsion. As shown in Fig. 1A, the device is assembled by joining two halves of a polydimethylsiloxane (PDMS) chip to allow for coaxial injection of the aqueous PEG hydrogel precursor into the continuous oil phase. The platform features three inlets—one for the oil phase, one for the cross-linking emulsion, and one for the aqueous phase—and a single outlet for droplet collection. The three phases remain separated until the convergence point at the flow-focusing junction.

The central aqueous channel has a square cross-section with a side of 320 μm to accommodate the passage of cell clusters, while each of the lateral oil/cross-linking emulsion channels has a rectangular cross-section, 400 μm wide and 460 μm high. Downstream of the junction, the gelation channel transitions to a rectangular cross-section, 800 μm wide and 460 μm high (Fig. 1B). All other dimensions are reported in Fig. S1. This design supports the transition of the aqueous phase from dripping to jetting regime with appropriate flow rate conditions, as illustrated schematically and experimentally in Fig. 1C. A real-time video showing the encapsulation process at the flow-focusing junction is available in SI (Video S1).

2.2 Microfluidic device fabrication and set up

The microfluidic device was designed through SolidWorks® software (Dassault Systèmes, SolidWorks Corporation, MA, USA). The desired features were milled using a computerized numerical control machine (Roland MDX-540, Roland DGA Corp, CA, USA) onto an optically transparent acrylic sheet (3.15 mm thick acrylic sheet from McMaster&Carr, Elmhurst, IL, USA) to fabricate the acrylic master mould. PDMS (SYLGARD™ 184 silicone elastomer kit: base and curing agent, Dow Corning, MI, USA) at a 10 : 1 w/w pre-polymer to curing agent ratio was used to produce two identical layers from the acrylic master mould, aligned and bonded together after a 50 second oxygen plasma treatment. Three Tygon® tubes (1.5 mm outer diameter, 0.5 mm inner diameter) were inserted into 1.5 mm inlet ports created using a 1.5 mm biopsy puncher (Integra Miltex, NJ, USA) and connected, *via* hypodermic needles (21G), to three syringes loaded with the solutions: one 1 mL glass Hamilton syringe for the aqueous phase and two 3 mL disposable syringes for the oil and cross-linking emulsion phases, respectively. Flow rates were controlled by three independent syringe pumps (PHD ULTRA syringe pump, Harvard Apparatus, MA, USA). The CC particulates were then collected in a 50 mL tube, pre-filled with cross-linking emulsion, through a Tygon® tube placed in a 4 mm outlet port, punched into the top PDMS layer using a 4 mm biopsy puncher (Integra Miltex).

2.3 Reagents preparation

2.3.1 Aqueous hydrogel precursor. A partially crosslinked (15%) 8-arm 10 kDa 75% functionalized PEG-maleimide (MAL) (JenKem, TX, USA) with 2 kDa PEG-dithiol (JenKem) in a 5 : 3 molar ratio (base : crosslinker) was used. Parameters were set to reach the optimal viscosity.[35] To allow even mixing and prevent instantaneous and heterogeneous gelation, the pH of this pre-polymer aqueous solution was lowered to 3 by adding 1 N hydrochloric acid (Millipore Sigma, MO, USA) and the temperature was controlled by keeping the pre-gel on ice. Before use, the pH was made neutral by adding small amounts of 1 N NaOH (Millipore Sigma).

2.3.2 Oil phase. The oil phase was composed of poly(propylene glycol) (PPG) (Millipore Sigma) and 10% Span80 surfactant (Millipore Sigma) to decrease the surface tension with the aqueous hydrogel precursor.

2.3.3 Cross-linking emulsion. The emulsion method involves the use of a PEG crosslinker water-in-oil emulsion to prompt gelation of the liquid gel precursor coating on the islets. The emulsion was prepared by adding 25 mg mL^{-1} molecular biology-grade DTT (VWR, PA, USA) in HBSS to the PPG/10% Span80 mixture.

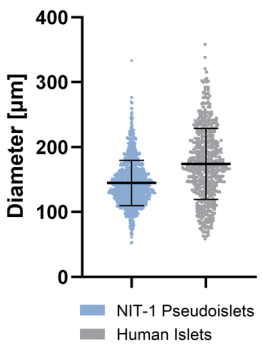

Fig. 2 Diameter distribution of NIT-1 pseudoislets and human islets. *N* = 1579 for NIT-1 pseudoislets and *N* = 537 for human islets. Diameters were manually measured on brightfield images using ImageJ software. Data are reported as median (NIT-1: 140.9 μm; HI: 170.9 μm) and interquartile range.

2.4 NIT-1 pseudoislet generation and culture

NIT-1 is a pancreatic β cell line derived from transgenic mouse insulinoma, proven to be a valid applicable model system for optimization and mechanistic studies in T1D.[52,53] As NIT-1 cells (ATCC, VA, USA) reached confluence in a 2D culture flask, the cells were transferred into a 30 mL spinner flask (ReproCELL, MD, USA) at a density of 1 million cells per mL and placed in the incubator on a magnetic stirrer plate rotating at a speed of 70 rpm until a median cluster diameter of 140.9 μm was reached (about 4 days) (Fig. 2).

The composition of culture media was the following: F-12K Medium (ATCC), 2 mM L-glutamine (Thermo Fisher, MA, USA), 10% FBS, 100 units per mL penicillin and 100 μg mL^{-1} of streptomycin (Thermo Fisher). For encapsulation, NIT-1 clusters were harvested from the spinner flasks and suspended in the PEG hydrogel precursor aqueous phase at a density of 160 IEQ mL^{-1}.

2.5 Human islet culture

Human islets (HI) were purchased from Prodo Laboratories Inc. (Aliso Viejo, CA, USA). Once received, the HI were moved to fresh media for 24 hours prior to use to permit recovery from the trauma of isolation and shipment. Composition of the media was as follows: PIM®, specifically formulated for culturing islets within the first 48 hours, is composed of 500 mL PIM®, 25 mL PIM(ABS)®, 5 mL PIM(G)®, 6 mL PIM(3X)®. HI population exhibited size heterogeneity, with a median diameter of 170.9 μm and an interquartile range of 136.1–210.3 μm (Fig. 2).

2.6 Experimental protocol

2.6.1 Encapsulation. The three Tygon® tubes were filled with the appropriate reagent solutions (PEG hydrogel precursor + cell clusters, oil phase, cross-linking emulsion) by setting the syringe pumps to infusion mode. While the tubes designated for the oil and cross-linking emulsion phases were directly connected to the respective inlets of the microfluidic chip, the tube for the aqueous phase required a preliminary loading step. Specifically, 40 μL of the aqueous hydrogel precursor containing the insulin-secreting cell clusters was first introduced into the tube pre-filled with mineral oil. To preserve cell viability and avoid exposure to high shear stress, the aqueous phase was withdrawn at a flow rate of 50 μL min^{-1}, allowing the cell clusters to enter the tubing directly—bypassing the needle. The encapsulation process and droplet formation were monitored in real time using a stereomicroscope (Motic SMZ-171, ES).

2.6.2 Purification. The process to isolate the encapsulated cells from the empty capsule and the oil phases began 12 minutes after collection in the 50 mL tube. 15 mL of mineral oil were added directly into the 50 mL tube containing the encapsulation product. Then, the 50 mL tube was filled with HBSS to the top, mixed by gently shaking, and centrifuged at 1500 rpm for 5 minutes. Two additional washes with HBSS were performed by centrifuging the conical tube at 1500 rpm for 5 minutes, aspirating up to 5 mL and refilling with HBSS.

The 5 mL pellet volume was transferred into a new 15 mL conical tube, rinsed, filled with HBSS, and spun at 1500 rpm for 5 minutes. The supernatant was aspirated, and the pellet incubated with 250 μL 1× PEG-dithiol for 1 minute, filled again with HBSS, and centrifuged at 1500 rpm for 1 minute. The supernatant was aspirated, 1 mL of media was added to resuspend the pellet, and centrifugation was performed at 250*g* for 3 minutes. After aspirating the supernatant, 15 mL of an islet gradient solution with a density of 1.037 g cm^{-3} density (Corning, NY, USA) was added, and the solution was centrifuged at 600*g* for 5 minutes with low brake.

After two washing cycles with 1 mL of media were carried out by centrifuging at 1000 rpm for 1 minute each, the sample was ready to be moved to a petri dish for further analysis.

2.6.3 Encapsulation parameters tested. Preliminary experiments were performed using polystyrene beads with diameters in the islet range (50–150 μm) at a concentration of 80 IEQ μL^{-1}, lower than the one used for encapsulating cell clusters, due to their rigidity and adhesive nature. These tests were carried out to narrow down the range of flow rates within which the water phase transitions from the dripping to the jetting regime. Subsequently, the flow rate combinations listed in Table 1 were tested using NIT-1 cell clusters.

2.7 Viability and functionality assessment

2.7.1 Thickness measurement. ImageJ (NIH, MD, USA) was used for quantitative analysis on brightfield images, measuring particle and capsule diameters, and capsule thickness on three different axes for each capsule.

2.7.2 GSIS protocol. GSIS was assessed the day after the encapsulation in both coated and uncoated cell clusters to evaluate insulin secretion in response to glucose challenges, a key feature of pancreatic islets for therapeutic applications. The assay was performed in a 24-well non-tissue-treated polystyrene plate, with transwells (Milicel, MA, USA). After a one-hour pre-incubation in low glucose solution (2.2 mM), clusters were sequentially incubated in (L1) low glucose (2.2 mM), (H) high glucose (16.6 mM), (L2) low glucose (2.2 mM), and (KCl) KCl solution (30 mM), each for one hour. Eluted samples were analyzed by insulin ELISA assay (Mercodia, SE).

2.7.3 Live/dead staining and confocal imaging. Cell viability was assessed using a live/dead assay. Samples were incubated at 37 °C for 1 hour in culture medium containing ethidium homodimer (1 : 1000), calcein AM (1 : 1000), and Hoechst (1 : 1000). Following incubation, three washing cycles were performed with HBSS. The samples were then transferred to a glass-bottom Petri dish for imaging, which was carried out using a Leica SP5 inverted confocal microscope (Leica Microsystems, DE). The acquired images were analyzed using Leica Application Suite or ImageJ software.

Table 1 Encapsulation parameters tested. Linear flow rates were calculated at the inlet channels of each phase, corresponding to cross-sections of 320 × 320 μm² for the aqueous phase and 400 × 460 μm² for the oil and cross-linking phases

Label	Aqueous phase flow rate [μL min⁻¹]	Oil phase flow rate [μL min⁻¹]	Cross-linking emulsion flow rate [μL min⁻¹]	Aqueous phase linear flow rate [μm s⁻¹]	Oil phase linear flow rate [mm s⁻¹]	Cross-linking emulsion linear flow rate [mm s⁻¹]
100 ; 100	3	100	100	488	9.0	9.0
140 ; 140	3	140	140	488	12.7	12.7
180 ; 180	3	180	180	488	16.3	16.3

2.7.4 Anti-PEG staining and confocal imaging. Samples were blocked and permeabilized in HBSS with 10% chicken serum and 0.2% Triton X-100 for 30 minutes, followed by 1 hour incubation with Rabbit Anti-PEG Antibody Biotin (1 : 500, AbCam, ab53449) in HBSS with 2% BSA. After washing, samples were incubated for 1 hour with streptavidin-conjugated AlexaFluor488 (1 : 200) and for 30 minutes with Hoechst (1 : 1000). Imaging was performed using a Leica SP5 inverted confocal microscope, and images were analyzed with Leica Application Suite or ImageJ software.

2.8 Statistical analysis

Data were elaborated using Excel, and statistical analysis was performed in GraphPad Prism 8 (GraphPad Software Inc., CA, USA). Normality of data distribution was assessed *via* the Shapiro–Wilk test. Differences between multiple groups were assessed using the Kruskal–Wallis test followed by Dunn's multiple comparisons *post hoc* test. Unpaired comparisons were evaluated using the Mann–Whitney *U* test. Correlation analyses were performed using Spearman's rank correlation. Significance was set at $p < 0.05$.

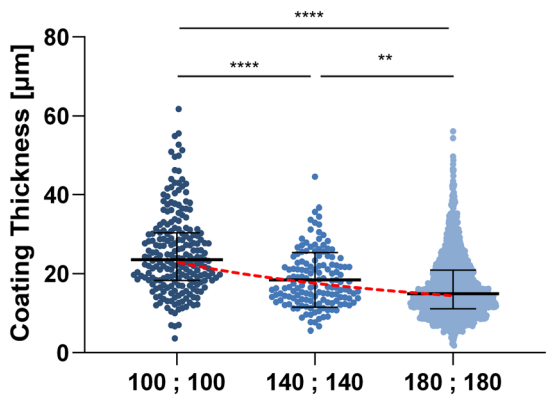

Fig. 3 Conformal coating (CC) thickness variation with oil phase flow rate. Measured CC thickness of encapsulated NIT-1 clusters *versus* oil phase flow rate (external oil phase flow rate; cross-linking emulsion phase flow rate). The flow rate of PEG hydrogel precursor is fixed at 3 μl min⁻¹. Thickness measurements were conducted using ImageJ by assessing capsule thickness along three orthogonal axes per capsule, and the mean value of these measurements is reported. Data are represented as median and interquartile range. $N = 4$ for 100 ; 100, $N = 1$ for 140 ; 140, $N = 20$ for 180; 180; $n > 100$ for each individual experiment. A fitted curve ($y = 903.03x^{-0.797}$) with $R^2 = 0.96$ is overlaid to illustrate the trend. $^{**}P < 0.01$; $^{****}P < 0.0001$ (Kruskal–Wallis test).

3 Results

To validate the performance of the microfluidic conformal coating platform, we conducted a comprehensive set of experiments using both NIT-1 clusters and primary human pancreatic islets.

3.1 Effects of oil phase flow rate on coating thickness

First, we evaluated the effects of changing the flow rates of the oil phase and the cross-linking emulsion phase on the conformal coating thickness using NIT-1 pseudoislets. Keeping the pseudoislet-containing aqueous hydrogel precursor flow rate constant, we found that the coating thickness decreased as the oil phase flow rate increased (Fig. 3). Specifically, a 40 μL min⁻¹ increase in both the oil and emulsion flow rates resulted in a marked reduction in coating thickness.

At an oil flow rate of 100 μL min⁻¹, the median coating thickness was 23.58 μm (first quartile (Q1) = 18.29 μm; third quartile (Q3) = 30.37 μm). Increasing the oil flow rate to 140 μL min⁻¹ reduced the median thickness to 16.58 μm (Q1 = 13.36 μm; Q3 = 22.40 μm), which was significantly different from the 100 μL min⁻¹ condition ($p < 0.0001$).

A further increase to 180 μL min⁻¹ yielded a median thickness of 14.89 μm (Q1 = 11.11 μm; Q3 = 20.88 μm), with significant differences observed when compared to both the 140 μL min⁻¹ ($p < 0.01$) and 100 μL min⁻¹ ($p < 0.0001$) conditions. The 180 ; 180 setting was chosen for further assessments due to its ability to consistently produce the thinnest hydrogel coatings among all presented conditions.

3.2 Validation of microfluidic platform for conformal coating of murine pseudoislets

NIT-1 cell clusters were encapsulated using flow rates of 3 μL min⁻¹ (clusters and hydrogel precursor solution), 180 μL min⁻¹ (oil phase), and 180 μL min⁻¹ (cross-linking emulsion) using our microfluidic platform (setting 180 ; 180), confirming qualitatively the conformality of the capsules (Fig. 4A). The NIT-1 clusters themselves exhibited a median diameter of 140.9 μm (Q1 = 121.2 μm; Q3 = 162.7 μm) (Fig. 2), highlighting a moderate degree of size heterogeneity. Capsule thickness ranged from a minimum of 1.81 μm to a maximum of 56.12 μm (Fig. 4B).

While capsule diameter exhibited a strong linear correlation with cluster diameter ($r = 0.87$) (Fig. 4C), capsule thickness remained independent of cluster size ($r = 0.09$)

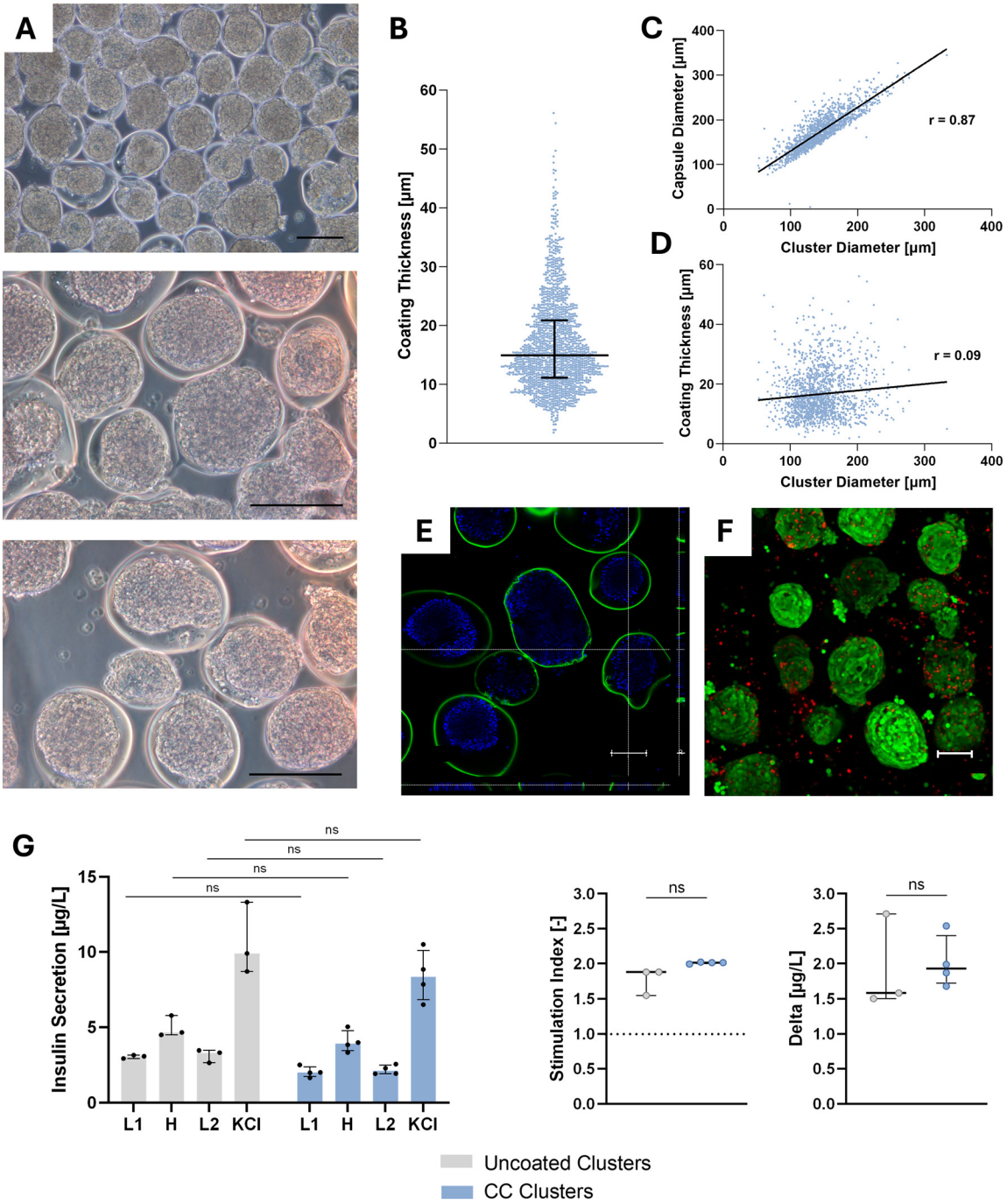

Fig. 4 Evaluation of conformal coating and functionality of encapsulated murine pseudoislets using the 180 ; 180 setting. (A) Representative phase contrast images of conformal coated (CC) NIT-1 insulinoma cell clusters at different magnifications across multiple independent experiments. Scale bars, 150 μm. The PEG hydrogel precursor was infused at a flow rate of 3 μl min^{-1}, while the external oil and the cross-linking emulsion were set at 180 μl min^{-1}. (B) Coating thickness measured from the NIT-1 cluster surface to the coating exterior. Each value represents the average of three measurements taken along three different axes. N = 20, with a total of n = 1579 clusters evaluated. Data are reported as median (14.89 μm) and interquartile range. (C) Correlation between cluster diameter and capsule diameter. Spearman correlation coefficient: r = 0.87 (R^2 = 0.76). Statistical significance: $P < 0.0001$. (D) Correlation between cluster diameter and coating thickness. Spearman correlation coefficient: r = 0.09 (R^2 = 0.01). Statistical significance: $P < 0.05$. (E) Capsule completeness shown as orthogonal projections of representative confocal images of anti-PEG (green) stained capsules (nuclei: blue). Scale bar, 100 μm. (F) Representative live/dead images (maximal intensity projection of 150 μm-thick z-stacks) of CC NIT-1 clusters 24 h after coating, shown as confocal images of live (green)/dead (red) stained cells (nuclei: blue). Scale bar, 100 μm. (G) GSIS functionality of uncoated (gray) and CC (light blue) NIT-1 clusters shown as insulin secretion (left), stimulation index (H/L1), and delta (H–L1) (right) during sequential stimulation with 2 mM glucose (L1), 16.7 mM glucose (H), 2 mM glucose (L2), and 30 mM KCl solutions. N = 3 independent batches of uncoated and N = 4 CC clusters, n = 3 technical replicates. Data are reported as median and interquartile range. Kruskal–Wallis test followed by Dunn's *post hoc* test was performed to analyze insulin secretion profile and Mann–Whitney test was performed on stimulation index and delta. ns: $P > 0.05$.

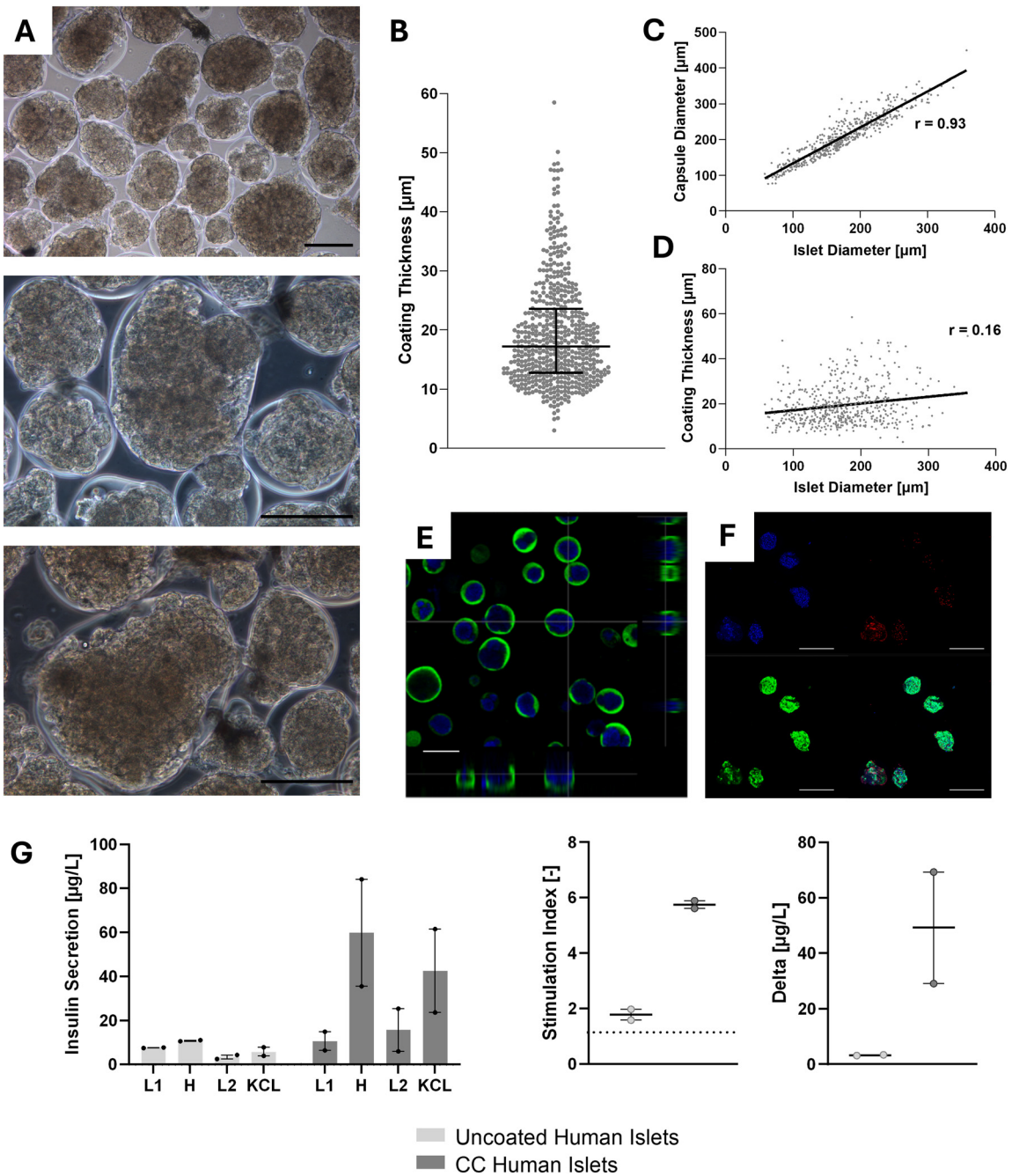

Fig. 5 Evaluation of conformal coating properties and functionality of primary human islets using the 180 ; 180 setting. (A) Representative phase-contrast images of conformal coated (CC) human islets (HI) at different magnifications across multiple independent experiments. Scale bars, 150 μm. (B) Coating thickness measured from the HI cluster surface to the coating exterior. Each value represents the average of three measurements taken along three different axes. N = 5, with a total of n = 537 islets evaluated. Data are reported as median (17.22 μm) and interquartile range. (C) Correlation between HI diameter and capsule diameter. Spearman correlation coefficient: r = 0.93 (R^2 = 0.86). Statistical significance: $P < 0.0001$. (D) Correlation between HI diameter and coating thickness. Spearman correlation coefficient: r = 0.16 (R^2 = 0.03). Statistical significance: $P < 0.05$. (E) Capsule completeness shown as orthogonal projections of confocal images of anti-PEG (green) stained capsules. Nuclei: blue. Scale bar, 150 μm. (F) Live/dead assessment of CC HI 24 h after coating shown as confocal images (maximal projection of 150 μm-thick z-stacks) of live (green)/dead (red) stained cells (nuclei: blue). Scale bar, 150 μm. (G) GSIS functionality of uncoated (light gray) and CC (dark gray) HI 24 h after encapsulation shown as insulin secretion (left), stimulation index (H/L1), and delta (H–L1) (right) during sequential stimulation with 2 mM glucose (L1), 16.7 mM glucose (H), 2 mM glucose (L2), and 30 mM KCl solutions. N = 2 independent batches of uncoated and CC islets and n = 3 technical replicates. Data are reported as median and interquartile range. The mean of the paired differences between coated and uncoated samples was 25.3 μg L^{-1} ± 20.5 μg L^{-1}.

(Fig. 4D), confirming the conformality of the encapsulation across different cluster dimensions.

Confocal images of CC NIT-1 clusters stained with Hoechst nuclear dye and anti-PEG antibody confirmed the completeness and integrity of the conformal coatings, where no significant cell protrusions outside the capsule could be identified (Fig. 4E). Live/dead staining revealed high viability of the clusters, with minimal presence of dead cells (Fig. 4F).

Both uncoated and CC NIT-1 clusters showed functional GSIS functionality (Fig. 4G). The CC clusters exhibited a stimulation index comparable to that of uncoated clusters (uncoated: median 1.880, interquartile range (IQR) 0.330; CC: median 2.013, IQR 0.021) and similar delta values (uncoated: median 1.585 μg L^{-1}, IQR 1.207 μg L^{-1}; CC: median 1.929 μg L^{-1}, IQR 0.675 μg L^{-1}).

3.3 Validation of microfluidic platform for conformal coating of primary human islets

Primary HI were encapsulated using the same flow rates as those used for NIT-1 cell cluster encapsulation (3 μL min^{-1} for clusters and hydrogel precursor solution; 180 μL min^{-1} for the oil phase; 180 μL min^{-1} for the cross-linking emulsion). HI coatings were comparable to NIT-1 coatings in terms of the capsules' adaptability to islet morphology (Fig. 5A). Quantitative analysis of capsule thickness revealed a median value of 17.22 μm (Q1 = 12.78 μm; Q3 = 23.58 μm), ranging from 3.01 μm to 55.51 μm (Fig. 5B).

The HI population exhibited a broader size distribution than NIT-1 clusters, with a median diameter of 170.9 μm (Q1 = 136.1 μm; Q3 = 210.3 μm), reflecting the natural heterogeneity of primary human islets (Fig. 2). Capsule diameter strongly correlated with islet diameter (r = 0.93) (Fig. 5C), while thickness remained largely independent (r = 0.16) (Fig. 5D), confirming coating conformality to islet shape and size. Confocal imaging of CC HI stained with Hoechst and anti-PEG antibody confirmed coating integrity and completeness (Fig. 5E). Live/dead staining revealed viable islets with only occasional dead cells (Fig. 5F).

GSIS assay (Fig. 5G) confirmed functional GSIS in both uncoated and CC HI. However, CC islets secreted substantially more insulin across all stimulation conditions, particularly under high glucose (16.6 mM) conditions, suggesting a protective effect of the hydrogel shell. Enhanced GSIS functionality of CC HI compared to uncoated HI was confirmed by a higher stimulation index (uncoated: median 1.783, IQR 0.395; CC: median 5.746, IQR 0.275) and insulin delta (uncoated: median 3.221 μg L^{-1}, IQR 0.282 μg L^{-1}; CC: median 49.22 μg L^{-1}, IQR 40.18 μg L^{-1}).

Notably, this difference in GSIS functionality was observed despite both groups containing comparable amounts of DNA (Fig. S2). However, statistical significance was not assessed due to the sample size. This observation suggests that the conformal coating may serve as a protective barrier, improving the well-being and functional maintenance of the encapsulated islet cells during *in vitro* culture after isolation.

4 Discussion

We developed a flow-focusing microfluidic platform that allows for conformal coating of insulin-secreting cell clusters with controllable thicknesses down to a few tens of micrometers, offering a simple, scalable, and tunable solution for islet microencapsulation in hydrogels. Compared to existing conformal coating strategies, our CC-on-chip approach avoids key limitations of both LbL and bulk emulsion methods. LbL coatings require direct modification of the islet cell surface and are inherently unstable due to membrane turnover,[34] while bulk emulsion-based systems lack precise control of coating thickness, expose islets to transient hypoxia in large external volumes, and do not allow real-time monitoring of the encapsulation process. By contrast, microfluidic systems are particularly well-suited for this application due to their low fabrication costs, reduced reagent consumption, and real-time control over flow dynamics. A key strength of the platform lies in its design flexibility: the geometry of every channel can be readily adapted to different sized cluster populations, for example going from small clusters to large spheroids by modifying the cross-sectional area of the clusters and hydrogel precursor solution to be >1.5-fold wider than the cell/clusters to encapsulate, and proportionally scaling up or down the size of the other channels, enabling rapid customization without major redesign. In addition, acrylic mould milling allow for fast and low-cost fabrication. This scalability is, however, bounded by the stability of the jetting regime and by gravity, which at larger dimensions begin to play a significant role in altering the jet and perturbing Plateau–Rayleigh breakup. Based on our estimates, the device can be practically scaled by approximately 5–7 times before gravitational effects become limiting.

Compared to the previous CC devices developed by our group,[23,35] the current platform offers a significantly faster and simpler setup. The duration of the encapsulation process itself is comparable between the two systems; however, downstream purification is faster in our workflow. In fact, although the same protocol is followed, the reduced reagent consumption associated with our device lowers the presence of residual oil phases, thereby decreasing the number of washing steps required. Importantly, our system also supports real-time monitoring of the encapsulation process, which is not possible with traditional CC setups, allowing immediate visual feedback and improved process control. Together, these improvements contribute to a more streamlined encapsulation process, well suited for both experimental and translational applications.

Fine-tuning the hydrogel coating thickness represents a critical engineering challenge, as it governs the balance between providing effective immunoprotection while preserving optimal mass transport dynamics necessary for sustained cell viability and function.[23,35] As demonstrated in Fig. 3, the increase of the oil phase and cross-linking emulsion flow rates resulted in a progressive reduction in

capsule thickness. This tunability is fundamental for optimizing the diffusion properties of the hydrogel shell and it provides a versatile approach to tailor encapsulation parameters based on specific clinical needs. Preliminary tests of the platform showed a high risk of leakage when applied flow rates approached 200 μL min^{-1}. To ensure operational stability, we thus limited the flow rates below this threshold for subsequent experiments; future work will focus on improving tubing connections to the PDMS chip to withstand higher pressures. Further, the aqueous hydrogel precursor containing the therapeutic cell clusters was maintained at a constant flow rate to keep the same encapsulation throughput, although it is also adjustable. Reducing the aqueous flow rate would have resulted in thinner coatings due to enhanced shear forces at the flow-focusing junction;[54,55] however, it would concurrently decrease the number of cell clusters encapsulated per unit of time. Conversely, rising the aqueous phase flow rate, although allowing for a higher encapsulation throughput rate, would produce thicker coatings and would increase the risk of compromising encapsulation uniformity and conformality. Empirical tests within a 1.5–5 μL min^{-1} range indicated that 3 μL min^{-1} represented the upper limit for maintaining coating conformality. Thus, the chosen flow rate setting reflects an optimized trade-off between achieving coating thickness within the desired range and preserving an efficient encapsulation rate. Importantly, the relative ratio between the aqueous and oil phase flow rates remains the key determinant for achieving consistent and conformal coatings, while preventing cluster aggregation or incomplete encapsulation. For more substantial adjustments of the coating thickness range, modifications to the microfluidic channel geometry can also be implemented with minimal design effort as discussed above.

All flow rate combinations we tested generated coatings with thickness in the desired range. However, the setting with oil phase and emulsion phases at 180 μL min^{-1} was selected for further experiments, as it consistently yielded the thinnest coatings. Specifically, compared to the 100 μL min^{-1} condition, this setting achieved a ~25% reduction in graft volume (considering that the median diameter of the NIT-1 cluster is 140.9 μm and assuming that the capsules are spherical), which is critical for translation of the encapsulation platform we report here to large numbers of human islets necessary for diabetes reversal in patients with T1D (~6% reduction compared to 140 ; 140). Although fluid-dynamic simulations could, in principle, provide mechanistic insights, applying them to this three-phase system with dynamic gelation would require major simplifications thereby limiting predictive power. Given the high computational cost of our previous two-phase models,[39] we opted for empirical optimization, which enabled robust and reproducible operating conditions.

Encapsulation results (Fig. 4 and 5) demonstrated that both NIT-1 insulinoma clusters and primary human islets were successfully conformally coated within a hydrogel shell thickness range compatible with nutrient and insulin diffusion. Quantitative analysis revealed a strong positive correlation between NIT-1 and HI cluster diameter and capsule diameter, and no correlation between capsule thickness and cluster size, confirming uniform coating across heterogeneous size clusters. Such consistency is particularly advantageous when dealing with cell clusters which naturally exhibit considerable size variability, such as primary human islets (HI diameter IQR: 74.2 μm; NIT-1 clusters diameter IQR: 41.5 μm).

Confocal imaging with anti-PEG staining demonstrated complete and uniform coverage of the clusters, with no major protrusions, supporting the conformality of the coating. Live/dead staining revealed high viability after encapsulation, and GSIS assays confirmed that both NIT-1 clusters and HI retained their functional insulin responsiveness to glucose challenge, indicating that shear forces during encapsulation did not substantially compromise islet integrity. This high viability of cell clusters after coating is further attributed to the fact that the encapsulation process maintains cells within a physiologically neutral pH environment throughout. Avoiding acidic or basic conditions during hydrogel polymerization is critical, as exposure to non-physiological pH has been associated with peripheral cell death, potentially triggering local inflammatory responses and compromising islet engraftment and survival upon transplantation.[35,51] Consistently, quantitative viability analysis confirmed ~96% viable cells in naked HI and ~81% in CC HI 24 h after encapsulation, indicating that a substantial fraction of islet cells remains viable after coating (Fig. S3); this early time point was chosen as it represents the clinically relevant window prior to transplantation, since extended *in vitro* culture of human islets is not informative due to their rapid loss of viability and function.[56]

In line with this, the preserved viability was reflected by functional performance, as CC HI exhibited improved GSIS functionality compared to uncoated controls, suggesting that the encapsulation not only preserved but may have enhanced islet functionality, although the small sample size precludes definitive conclusions. These results should be interpreted with caution, since apparent improvements in GSIS may reflect *in vitro* culture artefacts rather than intrinsic enhancement of islet function. From a translational standpoint, it is critical that coating does not diminish islet functionality, which our data confirm. Importantly, previous *in vivo* studies using the same PEG-based conformal coating demonstrated that coated islets maintained blood glucose regulation comparable to uncoated controls for up to 100 days, further supporting that the coating preserves islet function *in vivo*, due to the maintenance of diffusion distances within physiologically permissive ranges and the mitigation of hypoxia-related damage.[22,35] The enhanced insulin secretion was observed exclusively in primary HI, likely due to their greater sensitivity to environmental and mechanical stress compared to the more resilient NIT-1 pseudoislet model. In line with our findings, some studies

have reported a modest increase in insulin secretion following encapsulation, particularly during high-glucose stimulation phases,[35] while others observed no significant changes in secreted insulin levels after encapsulation.[57] Conversely, other reports have shown that encapsulation in alginate hydrogels may slightly impair GSIS responses.[21,23] These observations emphasize the importance of both capsule thickness and material properties in determining the functional outcome of islet encapsulation. Several mechanisms may underlie the observed functional enhancement: the capsule (i) could reduce exposure to mechanical and environmental stress during the GSIS assay, shielding the islets compared to uncoated controls; (ii) it may act as a physical spacer, preventing cluster adhesion to the culture substrate and promoting a more homogeneous distribution of oxygen and nutrients; (iii) may help maintain islet structural integrity, counteracting the tendency of isolated cells to disaggregate, preserving critical cell–cell communication and limiting the loss of supporting cells essential for islet functionality. In contrast, human islets microencapsulated with traditional methods have been reported to exhibit delayed and dampened insulin responses underscoring the advantage of CC in preserving physiological GSIS kinetics.[22] We acknowledge that we did not perform long-term culture of human islets, since extended *in vitro* maintenance is of limited relevance due to the rapid decline of viability and function of isolated islets.[56] Additionally, larger-scale studies are needed to confirm the functional benefits of conformal coating with sufficient statistical power, after which targeted experiments can clarify the contribution of individual mechanisms to the enhanced performance of primary islets. Thanks to this preliminary study, we were able to perform a power analysis based on the variance observed in the two available donors. The standard deviation of the paired differences was approximately 20 μg L^{-1}, while the mean difference was 25 μg L^{-1}. Under these assumptions, approximately 6–8 donors would be required to achieve 80–90% power at $\alpha = 0.05$. Beyond metabolic performance, previous studies with the same PEG-based conformal coatings have provided evidence of immunological protection and ongoing studies are confirming the stability of the hydrogel coatings over time, to demonstrate preservation of mechanical properties and diffusivity (unpublished data). In particular, Stock *et al.*[35] demonstrated that the hydrogel shell, while permeable to insulin and glucose with a diffusion velocity of 1110 ± 528 and 187 ± 89 $\mu m^2\ s^{-1}$, respectively, is impermeable to immunoglobulin G, a critical prerequisite for achieving immunoisolation. While the present study does not investigate immune mechanisms, these prior findings underscore that the microfluidic platform presented here builds upon an established foundation of immunological relevance.

In addition, the clinical applicability of this approach is particularly promising, given its potential to address several major limitations of current islet transplantation strategies. By enabling the generation of thin, conformal, and tunable hydrogel coatings, the microfluidic platform minimizes graft volume, facilitates transplantation into confined, highly vascularized, and potentially retrievable sites, and supports physiological glucose-insulin dynamics. Notably, conformal encapsulation with this system results in a graft volume that is 10- to 100-fold smaller than that required by conventional microencapsulation approaches to deliver the same number of islet equivalents.[19] This dramatic reduction greatly enhances the feasibility of transplantation into spatially constrained, highly vascularized sites such as the omental pouch[26] or the pre-vascularized subcutaneous site.[58,59] Furthermore, because conformal coating minimizes hypoxia-induced cell death by maintaining optimal diffusion distances and primary islet functionality through mechanisms still to be investigated, it may ultimately allow for the implantation of fewer IEQ while achieving comparable or superior therapeutic outcomes. In addition, the versatility and scalability of the device design make it adaptable to a broad range of therapeutic contexts beyond T1D, including other regenerative medicine applications where cell viability, function, and controlled engraftment are critical for clinical success.

While the system effectively produces conformal capsules with preserved cell viability and function, some limitations remain. Occasional protrusions in the hydrogel shell were observed, which may compromise the conformality of the coating and potentially reduce the effectiveness of immunoprotection. In this study, capsule integrity was assessed by anti-PEG staining, which cannot directly quantify potential cell protrusions. Staining of cell surface markers would allow a more accurate detection. Future studies should therefore explore direct cellular labeling approaches combined with quantitative image analysis. One possible solution to prevent uncoated protrusions is the implementation of a double-coating strategy, whereby cell clusters undergo a second passage through the microfluidic chip. This sequential approach can improve coating completeness and reduce surface irregularities, without introducing significant complexity to the process. Alternatively, refinements in the microfluidic chip design, particularly at the flow-focusing junction, may further improve coating consistency. For instance, replacing the current rectangular channel cross-sections with squared geometries at the junction has been shown to enhance the stability of the jet and may improve coating uniformity.[37] Such geometric refinements could contribute to more consistent coating formation and improved control over capsule morphology.

In terms of throughput, the current system enables an encapsulation rate of approximately 480 IEQ min^{-1}, which is three-fold lower than that of the previously reported non-chip-based conformal coating approach (~1500 IEQ min^{-1}). However, unlike the latter, our platform is readily scalable *via* parallelization. Thanks to its compact footprint and

low-cost fabrication, multiple devices can be operated in parallel to significantly increase the throughput, offering a practical path toward clinical-scale encapsulation. In fact, at this rate, coating a clinically relevant dose of about 700 000 IEQ (for a 70 kg recipient) would require about 24 h using a single chip, but operating for example 12 chips in parallel would reduce this time to about 2 h. By contrast, the previous macro-scale device, despite its higher throughput, would still require approximately 8 h to coat the same number of islets and could not be parallelized effectively, making our microfluidic platform substantially more suitable for clinical translation.

The compact and low-cost nature of the device, combined with its straightforward operation and minimal reagent use, underscores its potential as a prototype for a clinically usable, disposable cartridge. Such a design could be integrated into closed-loop workflows for automated islet encapsulation and consequent transplantation.

In conclusion, our flow-focusing microfluidic device demonstrates a robust, tuneable, and scalable platform for conformal hydrogel coating of pancreatic islets and insulin-secreting clusters, addressing major limitations of existing encapsulation technologies and paving the way for future clinical translation in regenerative medicine and T1D therapy.

Conclusions

We developed and validated a new flow-focusing microfluidic platform for the conformal hydrogel coating of insulin-secreting cell clusters, offering a streamlined, tuneable, and scalable alternative to conventional microencapsulation systems. By adjusting the flow rates of the immiscible phases, the platform reliably produced thin (10–20 μm) PEG hydrogel-based coatings with high uniformity and minimal reagent consumption. The system supported real-time monitoring of the process and was adaptable to both murine NIT-1 pseudoislets and to primary human islets, preserving cell viability and GSIS functionality.

Compared to previously reported conformal coating methods, this microfluidic platform simplifies device handling, and allows for straightforward redesign for application customization and scalability through parallelization—critical for translating cell-based therapies into clinical use.

While this study focused on encapsulation of insulin-secreting cell clusters for T1D, the technology is readily adaptable to other cell types and therapeutic contexts where immune isolation, minimal transplant volume, and sustained cell function are essential. Overall, this microfluidic platform offers a practical and versatile foundation for advancing and translating conformal encapsulation strategies in regenerative medicine. This work thus represents not only a robust microfluidic platform for islet encapsulation, but also a compelling proof of concept for a future disposable cartridge system tailored for clinical translation.

Author contributions

Methodology: FV, TM, FV, GCG; investigation: FV, TM, FV, HM; visualization: FV, TM, FV, GCG, HM, SB, AA, MR, AR, AAT; funding acquisition: AAT; project administration: AAT, AR; supervision: FV, TM, AA, AR, AAT; writing – original draft: FV, TM; writing – review & editing: AAT, AR, GCG, MR; conceptualization: AR, AAT, MR.

Conflicts of interest

AAT is an inventor of the IP used in the studies and licensed to Sernova Corp. AAT has received payment from Sernova related to the IP and stand to gain royalties from commercialization of the IP. Additionally, AAT is an equity holder in Sernova Corp. The authors declare no other competing interests.

Data availability

The data that support the findings of this study are available from the corresponding author upon reasonable request.

Supplementary information: Fig. S1–S3 and Video S1. See DOI: **https://doi.org/10.1039/d5lc00690b**.

Acknowledgements

Funding for this work was provided by the Diabetes Research Institute Foundation, the National Institutes of Health (NIH) National Institute of Diabetes and Digestive and Kidney Diseases (NIDDK) grant 1 and 2 R01DK109929 (AAT), and Breakthrough T1D (ex JDRF) (grants 5-CDA-2016-171-S-B (AAT)). This work was funded by the National Plan for NRRP Complementary Investments (PNC, established with the decree-law 6 May 2021, no. 59, converted by law no. 101 of 2021) in the call for the funding of research initiatives for technologies and innovative trajectories in the health and care sectors (Directorial Decree no. 931 of 06-06-2022) – project no. PNC0000003 – Advanced Technologies for Human-centred Medicine (project acronym: ANTHEM) (AR). This work reflects only the authors' views and opinions, neither the Ministry for University and Research nor the European Commission can be considered responsible for them.

Notes and references

1 T. B. Lopez-Mendez, E. Santos-Vizcaino, J. L. Pedraz, G. Orive and R. M. Hernandez, *J. Controlled Release*, 2021, **335**, 619–636.
2 L. Xuan, Y. Hou, L. Liang, J. Wu, K. Fan, L. Lian, J. Qiu, Y. Miao, H. Ravanbakhsh, M. Xu and G. Tang, *Microgels for Cell Delivery in Tissue Engineering and Regenerative Medicine*, Springer Nature Singapore, 2024, vol. 16, pp. 1–42.
3 B. Farasati Far, M. Safaei, R. Nahavandi, A. Gholami, M. R. Naimi-Jamal, S. Tamang, J. E. Ahn, M. Ramezani Farani and Y. S. Huh, *ACS Omega*, 2024, **9**, 29139–29158.

4 T. Alkayyali, T. Cameron, B. Haltli, R. G. Kerr and A. Ahmadi, *Anal. Chim. Acta*, 2019, **1053**, 1–21.
5 S. Y. Lee, J. Ma, T. S. Khoo, N. Abdullah, N. N. F. Nik Md Noordin Kahar, Z. A. Abdul Hamid and M. Mustapha, *Front. Bioeng. Biotechnol.*, 2021, **9**, 1–19.
6 A. Katsarou, S. Gudbjörnsdottir, A. Rawshani, D. Dabelea, E. Bonifacio, B. J. Anderson, L. M. Jacobsen, D. A. Schatz and A. Lernmark, *Nat. Rev. Dis. Primers*, 2017, **3**, 1–18.
7 L. A. DiMeglio, C. Evans-Molina and R. A. Oram, *Lancet*, 2019, **176**, 139–148.
8 A. Rech Tondin and G. Lanzoni, *BioDrugs*, 2025, **39**, 261–280.
9 T. Anazawa, S. Marubashi, S. Kodama, M. Goto, M. Maruyama, H. Eguchi, M. Shimoda, H. Noguchi, T. Yamaguchi, T. Ito, T. Kenmochi and M. Gotoh, *Transplant. Direct*, 2025, **11**, e1765.
10 B. A. Marfil-Garza, J. Hefler, K. Verhoeff, A. Lam, K. Dajani, B. Anderson, D. O'Gorman, T. Kin, O. Y. Bello-Chavolla, D. Grynoch, A. Halpin, P. M. Campbell, P. A. Senior, D. Bigam and A. M. Shapiro, *Ann. Surg.*, 2023, **277**, 672–680.
11 B. J. Hering, M. R. Rickels, M. D. Bellin, J. R. Millman, A. A. Tomei, A. J. García, H. Shirwan, C. L. Stabler, M. Ma, P. Yi, X. Luo, Q. Tang, S. Ramachandran, J. Oberholzer, C. Ricordi, T. J. Kieffer and A. M. J. Shapiro, *Diabetes*, 2025, **74**(7), 1068–1077.
12 A. Grattoni, G. Korbutt, A. A. Tomei, A. J. García, A. R. Pepper, C. Stabler, M. Brehm, K. Papas, A. Citro, H. Shirwan, J. R. Millman, J. Melero-Martin, M. Graham, M. Sefton, M. Ma, N. Kenyon, O. Veiseh, T. A. Desai, M. C. Nostro, M. Marinac, M. Sykes, H. A. Russ, J. Odorico, Q. Tang, C. Ricordi, E. Latres, N. E. Mamrak, J. Giraldo, M. C. Poznansky and P. de Vos, *Nat. Rev. Endocrinol.*, 2024, **21**, 14–30.
13 A. M. Shapiro, M. Pokrywczynska and C. Ricordi, *Nat. Rev. Endocrinol.*, 2017, **13**, 268–277.
14 M. D. Bellin, F. B. Barton, A. Heitman, R. Alejandro and B. J. Hering, *Bone*, 2013, **23**, 1–7.
15 M. Farina, J. F. Alexander, U. Thekkedath, M. Ferrari and A. Grattoni, *Adv. Drug Delivery Rev.*, 2019, **139**, 92–115.
16 S. N. Marikar, A. El-Osta, A. Johnston, G. Such and K. Al-Hasani, *Cell. Mol. Life Sci.*, 2022, **79**, 1–13.
17 M. Köllmer, A. A. Appel, S. I. Somo and E. M. Brey, *Tissue Eng., Part B*, 2016, **22**, 34–46.
18 M. D. Bellin and T. B. Dunn, *Diabetologia*, 2020, **63**, 2049–2056.
19 S. Kioulaphides and A. J. García, *Adv. Drug Delivery Rev.*, 2024, **207**, 1–40.
20 L. A. Llacua, M. M. Faas and P. de Vos, *Diabetologia*, 2018, **61**, 1261–1272.
21 P. Buchwald, A. Tamayo-Garcia, V. Manzoli, A. A. Tomei and C. L. Stabler, *Biotechnol. Bioeng.*, 2019, **115**, 232–245.
22 T. De Toni, A. A. Stock, F. Devaux, G. C. Gonzalez, K. Nunez, J. C. Rubanich, S. A. Safley, C. J. Weber, N. M. Ziebarth, P. Buchwald and A. A. Tomei, *Front. Bioeng. Biotechnol.*, 2022, **10**, 1–16.
23 A. A. Tomei, V. Manzoli, C. A. Fraker, J. Giraldo, D. Velluto, M. Najjar, A. Pileggi, R. D. Molano, C. Ricordi, C. L. Stabler and J. A. Hubbell, *Proc. Natl. Acad. Sci. U. S. A.*, 2014, **111**, 10514–10519.
24 T. Qin, A. M. Smink and P. de Vos, *Acta Biomater.*, 2023, **167**, 38–53.
25 D. M. Berman, R. D. Molano, C. Fotino, U. Ulissi, J. Gimeno, A. J. Mendez, N. M. Kenyon, N. S. Kenyon, D. M. Andrews, C. Ricordi and A. Pileggi, *Diabetes*, 2016, **65**, 1350–1361.
26 D. A. Baidal, C. Ricordi, D. M. Berman, A. Alvarez, N. Padilla, G. Ciancio, E. Linetsky, A. Pileggi and R. Alejandro, *N. Engl. J. Med.*, 2017, **176**, 100–106.
27 M. Najjar, V. Manzoli, M. Abreu, C. Villa, M. M. Martino, R. D. Molano, Y. Torrente, A. Pileggi, L. Inverardi, C. Ricordi, J. A. Hubbell and A. A. Tomei, *Biotechnol. Bioeng.*, 2015, **112**, 1916–1926.
28 Y. Fukuda, T. Akagi, T. Asaoka, H. Eguchi, K. Sasaki, Y. Iwagami, D. Yamada, T. Noda, K. Kawamoto, K. Gotoh, S. Kobayashi, M. Mori, Y. Doki and M. Akashi, *Biomaterials*, 2018, **160**, 82–91.
29 H. Park, M. R. Haque, J. B. Park, K. W. Lee, S. Lee, Y. Kwon, H. S. Lee, G. S. Kim, D. Y. Shin, S. M. Jin, J. H. Kim, H. J. Kang, Y. Byun and S. J. Kim, *Biomaterials*, 2018, **171**, 164–177.
30 K. M. Gattas-Asfura and C. L. Stabler, *ACS Appl. Mater. Interfaces*, 2013, **23**, 1–7.
31 W. Li, X. Lei, H. Feng, B. Li, J. Kong and M. Xing, *Pharmaceutics*, 2022, **14**, 1–27.
32 Q. Zhang, C. Gonelle-Gispert, Y. Li, Z. Geng, S. Gerber-Lemaire, Y. Wang and L. Buhler, *Front. Immunol.*, 2022, **13**, 1–16.
33 M. R. Haque, J. Kim, H. Park, H. S. Lee, K. W. Lee, T. A. Al-Hilal, J. H. Jeong, C. H. Ahn, D. S. Lee, S. J. Kim and Y. Byun, *J. Controlled Release*, 2017, **258**, 10–21.
34 A. Opara, A. Jost, S. Dagogo-Jack and E. C. Opara, *Exp. Biol. Med.*, 2021, **246**, 2570–2578.
35 A. A. Stock, G. C. Gonzalez, S. I. Pete, T. De Toni, D. M. Berman, A. Rabassa, W. Diaz, J. C. Geary, M. Willman, J. M. Jackson, N. H. DeHaseth, N. M. Ziebarth, A. R. Hogan, C. Ricordi, N. S. Kenyon and A. A. Tomei, *Sci. Adv.*, 2022, **8**, 1–15.
36 A. A. Stock, V. Manzoli, T. De Toni, M. M. Abreu, Y. C. Poh, L. Ye, A. Roose, F. W. Pagliuca, C. Thanos, C. Ricordi and A. A. Tomei, *Stem Cell Rep.*, 2020, **14**, 91–104.
37 J. K. Nunes, S. S. H. Tsai, J. Wan and H. A. Stone, *J. Phys. D: Appl. Phys.*, 2013, **23**, 1–7.
38 E. Castro-Hernández, V. Gundabala, A. Fernández-Nieves and J. M. Gordillo, *New J. Phys.*, 2009, **11**, year.
39 S. Sibilla, S. Manenti, T. Cazzato, F. Colombo, A. A. Tomei, A. Redaelli, V. Manzoli and F. Consolo, *Med. Eng. Phys.*, 2020, **176**, 139–148.
40 A. A. Tomei, A. Stock and M. Lupp, Conformal coating of cells for immunoisolation, *Int. Pat.*, WO2021/222469A1, 2021.
41 C. Ricordi, D. W. Gray, B. J. Hering, D. B. Kaufman, G. L. Warnock, N. M. Kneteman, S. P. Lake, N. J. London, C. Socci, R. Alejandro, Y. Zeng, D. W. Scharp, G. Viviani, L. Falqui, A. Tzakis, R. G. Bretzel, K. Federlin, G. Pozza, R. F. James, R. V. Rajotte, V. D. Carlo, P. J. Morris, D. E. Sutherland, T. E. Starzl, D. H. Mintz and P. E. Lacy, *Acta Diabetol. Lat.*, 1990, **27**, 185–195.

42 J. F. Markmann, S. Deng, X. Huang, N. M. Desai, E. H. Velidedeoglu, C. Lui, A. Frank, E. Markmann, M. Palanjian, K. Brayman, B. Wolf, E. Bell, M. Vitamaniuk, N. Doliba, F. Matschinsky, C. F. Barker, A. Naji, J. A. Haller, H. Shokouh-Amiri, N. M. Kenyon, W. C. Chapman, F. C. Brunicardi and J. F. Markmann, *Ann. Surg.*, 2003, **237**, 741–750.

43 K. A. White, R. Chalaby and R. Olabisi, *Regener. Eng. Transl. Med.*, 2022, **8**, 345–354.

44 D. M. Headen, G. Aubry, H. Lu and A. J. García, *Adv. Mater.*, 2014, **26**, 3003–3008.

45 C. Kim, S. Chung, Y. E. Kim, K. S. Lee, S. H. Lee, K. W. Oh and J. Y. Kang, *Lab Chip*, 2011, **11**, 246–252.

46 S. Köster, F. E. Angilè, H. Duan, J. J. Agresti, A. Wintner, C. Schmitz, A. C. Rowat, C. A. Merten, D. Pisignano, A. D. Griffiths and D. A. Weitz, *Lab Chip*, 2008, **8**, 1110–1115.

47 C. H. Choi, J. H. Jung, Y. W. Rhee, D. P. Kim, S. E. Shim and C. S. Lee, *Biomed. Microdevices*, 2007, **9**, 855–862.

48 F. Shao, L. Yu, Y. Zhang, C. An, H. Zhang, Y. Zhang, Y. Xiong and H. Wang, *Front. Bioeng. Biotechnol.*, 2020, **8**, 1–13.

49 A. Sattari, S. Janfaza, M. Mashhadi Keshtiban, N. Tasnim, P. Hanafizadeh and M. Hoorfar, *ACS Omega*, 2021, **6**, 25964–25971.

50 H. Shieh, M. Saadatmand, M. Eskandari and D. Bastani, *Sci. Rep.*, 2021, **11**, 1–10.

51 S. Nagata, R. Hanayama and K. Kawane, *Cell*, 2010, **140**, 619–630.

52 K. Hamaguchi, H. R. Gaskins and E. H. Leiter, *Diabetes*, 1991, **40**, 842–849.

53 G. C. Gonzalez, C. M. Li, I. Pasolini, S. I. Pete, C. Verheyen, S. M. Vignolo, T. De Toni, A. A. Stock and A. A. Tomei, *Cell. Transplant.*, 2025, **34**, 1–22.

54 A. M. Ibrahim, J. I. Padovani, R. T. Howe and Y. H. Anis, *Micromachines*, 2021, **12**, 1–11.

55 A. Lashkaripour, C. Rodriguez, L. Ortiz and D. Densmore, *Lab Chip*, 2019, **19**, 1041–1053.

56 R. Lehmann, R. A. Zuellig, P. Kugelmeier, P. B. Baenninger, W. Moritz, A. Perren, P. A. Clavien, M. Weber and G. A. Spinas, *Diabetes*, 2007, **56**, 594–603.

57 F. Syed, M. Bugliani, M. Novelli, F. Olimpico, M. Suleiman, L. Marselli, U. Boggi, F. Filipponi, V. Raffa, S. Krol, D. Campani, P. Masiello, V. De Tata and P. Marchetti, *Nanomed.: Nanotechnol., Biol. Med.*, 2018, **14**, 2191–2203.

58 B. Keymeulen, K. De Groot, D. Jacobs-Tulleneers-Thevissen, D. M. Thompson, M. D. Bellin, E. J. Kroon, M. Daniels, R. Wang, M. Jaiman, T. J. Kieffer, H. L. Foyt and D. Pipeleers, *Nat. Biotechnol.*, 2023, **42**, 1507–1514.

59 Sernova Corp, *A Safety, Tolerability and Efficacy Study of Sernova's Cell Pouch™ for Clinical Islet Transplantation*, 2018, **https://clinicaltrials.gov/ct2/show/NCT03513939?term=NCT03513939&draw=2&rank=1**.